

Band alignment tuning in diamond (100)/CNT heterostructures via surface passivation: First-principles design for high-power nanoelectronics

Linan Ma(马利南), Rui Ma(马锐), Jieyi Huang(黄婕伊), Yongsheng Yao(姚永胜), Tao Ouyang(欧阳滔), Juexian Cao(曹觉先), and Xiaolin Wei(魏晓林)

Citation: Chin. Phys. B, 2026, 35 (**8**): 087301. DOI: 10.1088/1674-1056/ae1453
http://cpb.iphy.ac.cn; http://iopscience.iop.org/cpb

What follows is a list of articles you may be interested in

Band alignment of heterojunctions formed by $PtSe_2$ with doped GaN

Zhuoyang Lv(吕卓阳), Guijuan Zhao(赵桂娟), Wanting Wei(魏婉婷), Xiurui Lv(吕秀睿), and Guipeng Liu(刘贵鹏)
Chin. Phys. B, 2025, 34 (**4**): 047304. DOI: 10.1088/1674-1056/adb67b

Interface engineering of transition metal dichalcogenide/GaN heterostructures: Modified broadband for photoelectronic performance

Yinlu Gao(高寅露), Kai Cheng(程开), Xue Jiang(蒋雪), and Jijun Zhao(赵纪军)
Chin. Phys. B, 2022, 31 (**11**): 117304. DOI: 10.1088/1674-1056/ac6eee

Band alignment of p-type oxide/ε-Ga_2O_3 heterojunctions investigated by x-ray photoelectron spectroscopy

Chang Rao(饶畅), Zeyuan Fei(费泽元), Weiqu Chen(陈伟驱), Zimin Chen(陈梓敏), Xing Lu(卢星), Gang Wang(王钢), Xinzhong Wang(王新中), Jun Liang(梁军), Yanli Pei(裴艳丽)
Chin. Phys. B, 2020, 29 (**9**): 097303. DOI: 10.1088/1674-1056/ab9c0d

Energy band alignment at Cu_2O/ZnO heterojunctions characterized by *in situ* x-ray photoelectron spectroscopy

Yan Zhao(赵妍), Hong-Bu Yin(尹泓卜), Ya-Jun Fu(符亚军), Xue-Min Wang(王雪敏), Wei-Dong Wu(吴卫东)
Chin. Phys. B, 2019, 28 (**8**): 087301. DOI: 10.1088/1674-1056/28/8/087301

Conductivity and band alignment of $LaCrO_3$/$SrTiO_3$ (111) heterostructure

Yan-Peng Hong(洪彦鹏), Xin-Xin Wang(王欣欣), Guo-Liang Qu(曲国良), Cheng-Jian Li(厉承剑), Hong-Xia Xue(薛红霞), Ke-Jian Liu(刘科践), Yong-Chun Li(李永春), Chang-Min Xiong(熊昌民), Rui-Fen Dou(窦瑞芬), Lin He(何林), Jia-Cai Nie(聂家财)
Chin. Phys. B, 2018, 27 (**4**): 047301. DOI: 10.1088/1674-1056/27/4/047301

Band alignment tuning in diamond (100)/CNT heterostructures via surface passivation: First-principles design for high-power nanoelectronics

Linan Ma(马利南)[1,†], Rui Ma(马锐)[1,4,†], Jieyi Huang(黄婕伊)[1], Yongsheng Yao(姚永胜)[2], Tao Ouyang(欧阳滔)[1], Juexian Cao(曹觉先)[1,3], and Xiaolin Wei(魏晓林)[1,2,‡]

[1] *Department of Physics & Hunan Institute of Advanced Sensing and Information Technology, Xiangtan University, Xiangtan* 411105, *China*
[2] *College of Physics and Electronics Engineering, Hengyang Normal University, Hengyang* 421002, *China*
[3] *Hunan Provincial Key Laboratory of Smart Carbon Materials and Advanced Sensing, Xiangtan University, Xiangtan* 411105, *China*
[4] *College of Physics Science and Engineering Technology, Yichun University, Yichun* 336000, *China*

(Received 27 August 2025; revised manuscript received 17 October 2025; accepted manuscript online 17 October 2025)

Benefiting from the high electron mobility and ultra-thin geometric features, carbon nanotubes (CNTs) exhibit great potential as semiconductor channel materials in micro/nano electronic devices. Diamond (Dia), with superior hardness and chemical inertness, is an ideal substrate material for CNT-based electronic devices. In this study, using first-principles calculations, we systematically investigate the effect of surface reconstruction and passivation on the electronic structure of the heterojunction formed by the Dia (100) surface and CNT, as well as the associated band alignment at the interface. Our calculations indicate that surface reconstruction and passivation treatments could facilitate the formation of a type-I heterojunction between Dia (100) and CNT, which meets the performance criteria required for CNT-based electronic applications. More importantly, oxygen passivation could result in both the conduction band offset (CBO) and valence band offset (VBO) between Dia (100) and CNT being greater than 1.0 eV. The findings presented in this work demonstrate the critical role of surface reconstruction and passivation in enhancing the performance of CNT-based high-performance radio frequency (RF) and optoelectronic devices. They also provide valuable insights for optimizing CNT field-effect transistor (FET) interfaces.

Keywords: diamond (100), 1D/3D van der Waals heterostructures, band offset

PACS: 73.22.–f, 71.15.Mb, 73.20.At, 73.21.Hb

DOI: 10.1088/1674-1056/ae1453 **CSTR:** 32038.14.CPB.ae1453

1. Introduction

Advanced integrated circuit technologies urgently require novel channel materials to address the challenges arising from power consumption and heat dissipation. Low-dimensional semiconductor materials, especially carbon nanotubes (CNTs), with high mobility and ultra-thin geometric features, host theoretical advantages in performance, energy efficiency, and miniaturization capabilities.[1–3] Recent breakthroughs in the fabrication of CNT arrays with ultra-high semiconductor purity and high density have enabled the development of high-speed radio frequency (RF) transistors and ultra-miniaturized digital logic transistors, also endowing CNTs with practical advantages in next-generation micro/nano devices.[4–6] It is well known that substrate materials play a critical role in electronic devices. Silicon is widely used as a substrate for CNT-based field-effect transistors (CNT-FETs).[7–9] However, silicon's sensitivity to external factors, such as temperature and radiation, limits the device performance.[10] Meanwhile, the inherent defects and impurities in silicon could also lead to significant interface states, thereby hindering carrier transport.[11–13] Consequently, exploring suitable substrate materials to optimize the interface and stability of CNT-based electronic devices is crucial for enhancing the performance.

Benefiting from its ultra-wide bandgap, high carrier mobility, and high critical breakdown electric field, diamond (Dia) is regarded as the ultimate semiconductor material for electronic devices.[14,15] The high stability and low defect density of diamond also make it very suitable as a substrate material to maximize the performance of CNTs.[16–18] Meanwhile, owing to their intrinsic one-dimensional and three-dimensional geometric characteristics, Dia/CNT composites are expected to host advantages in performance enhancement, power consumption reduction, and integration.[19–22] When CNTs and Dia form a heterojunction, there are multiple crystal plane options. Among these various crystal planes, the Dia (100) surface stands out because of the lower surface roughness, along with fewer defects and impurities.[23–25] Therefore, the Dia (100) surface is the ideal choice as a substrate material for CNT-based devices.[26–29] Notably, an

[†] These authors contributed equally to this work.
[‡] Corresponding author. E-mail: xlw@xtu.edu.cn
© 2026 Chinese Physical Society and IOP Publishing Ltd. All rights, including for text and data mining, AI training, and similar technologies, are reserved.

interfacial band offset greater than 1.0 eV is essential for device performance enhancement.[30–32] However, the pristine Dia (100)/CNT heterojunction might not meet such requirements.[33] Accordingly, in order to design and optimize Dia/CNT electronic devices, it is necessary to investigate the effects of reconstruction and passivation on the energy band structure of this heterojunction.

Motivated by the above statements, by means of first-principles calculations based on density-functional theory (DFT),[34,35] we systematically investigate the electronic structure and energy band alignment of heterostructures formed by Dia (100) surfaces and CNTs. The results show that passivation and reconstruction can effectively modify the band structure of diamond, thereby inducing significant adaptations in the band alignment of Dia (100)/CNT heterostructures. Meanwhile, it is found that different passivation types can significantly modulate the electronic properties at the interface. The CNTs lose electrons when passivated with F, O, or OH, whereas they gain electrons under H-passivation. The remainder of the paper is organized as follows. In the next section, the calculation details are briefly described. In Section 3, we systematically analyze the correction results of the two structures under different passivation conditions and identify the O-passivated diamond surface as the optimal configuration meeting the requirements for device applications. Finally, a comprehensive summary of our conclusions is provided in Section 4.

2. Methods

In this work, all calculations are performed within the framework of the generalized gradient approximation (GGA) of density functional theory (DFT) as implemented in Vienna *Ab-initio* Simulation Package (VASP).[34–37] Valence electrons are described using a plane-wave basis set within the projector augmented wave (PAW) method.[38] The DFT-D3 correction is applied to account for van der Waals interactions.[39] To ensure decoupling between adjacent layers, a vacuum layer of 20-Å thickness is introduced along the z-direction. The plane-wave cutoff energy is set to 500 eV, and both lattice constants and atomic positions are fully optimized utilizing the conjugate gradient algorithm. A $4\times1\times1$ Monkhorst–Pack k-point grid is used for sampling the Brillouin zone.[40,41] The structure is relaxed until the maximum force on each atom is below a convergence threshold of 0.01 eV Å^{-1}, with a total energy convergence criterion of 10^{-5} eV. Finally, the electronic structure is corrected using the high-accuracy HSE06 functional.[42,43]

3. Results and discussion

Due to the similar lattice constants, we constructed a heterojunction formed by (6,2)-CNT and Dia (100)-2×2 reconstructed surface. The effect of interface orientations on the binding energy and electronic structure of this heterojunction is first investigated. Here, the binding energy is defined as

$$E_{\mathrm{b}} = \frac{E_{\mathrm{Dia-CNT}} - E_{\mathrm{Dia}} - E_{\mathrm{CNT}}}{L_{\mathrm{CNT}}}, \tag{1}$$

where $E_{\mathrm{Dia-CNT}}$ represents the energy of the heterojunction, E_{Dia} denotes the energy of the Dia, E_{CNT} is the energy of the CNT, and L_{CNT} is the length of the CNT. In this work, we mainly consider two orientations, *i.e.*, parallel and perpendicular to the channel direction. The corresponding structures are shown in Fig. S1 of the supporting material. The calculations indicate that the heterojunction constructed along the channel direction holds a lower binding energy (-5×10^{-3} eV/Å) compared to that along the perpendicular direction (-4.9×10^{-3} eV/Å). However, as for the electronic properties, the two construction orientations have only a slight impact on the electronic band structure, with no significant changes in the bandgap or charge distribution (see Fig. S2 in the supporting materials). From the perspective of binding energy, we will focus on the heterojunction constructed along the channel direction in subsequent studies. Additionally, we constructed a heterojunction formed by the (8,0)-CNT and the Dia (100)-2×1 reconstructed surface, which exhibits a lattice mismatch of 0.9%. By analyzing the binding energies and electronic properties of these two structural models with different degrees of lattice matching, we can effectively verify the universality and consistency of the results. The reconstructed Dia (100) surface has numerous dangling bonds. To address this, we use different functional groups to passivate the surface and study their effects on the electronic properties. Figure 1 depicts the heterostructure with fluorine (F) passivation, while Fig. S3 in the supporting materials shows the

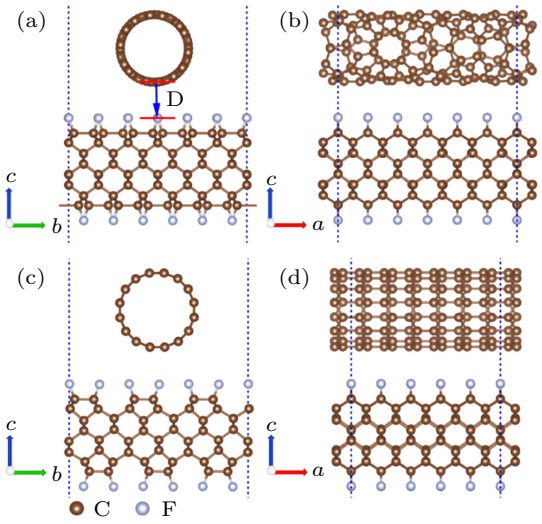


Fig. 1. (a) and (b) Side views of the heterojunction formed by Dia (100)-2×2 reconstruction and a (6,2) carbon nanotube. (c) and (d) Side views of the heterojunction formed by Dia (100)-2×1 reconstruction and a (8,0) carbon nanotube. Brown spheres represent carbon atoms, and blue spheres represent fluorine atoms.

heterostructures with oxygen (O), hydroxyl (OH), and hydrogen (H) passivation. In Fig. 1(a), the label D indicates the distance between the F-passivated atoms on the surface and the CNT. The interatomic distances for atoms passivated with other functional groups are listed in Table 1. The binding energy, charge transfer, interfacial distance, and bandgap for all constructed heterostructures were calculated, and the results are presented in Table 1.

Table 1. Binding energy, charge transfer, interatomic distance between the CNT and Dia, and bandgap for the Dia (100)-2 × 1 reconstruction & (8,0) CNT under four different passivation conditions.

Structure	E_b (eV/Å)	Bader–CNT (*e*/nm)	Distance (Å)	Band gap (eV)
2 × 1F/ (8,0) CNT	–0.207	–0.052	3.15	0.66
2 × 1-O/ (8,0) CNT	0.206	0.006	2.99	0.65
2 × 1-OH/ (8,0) CNT	0.199	0.017	3.23	0.48
2 × 1-H/ (8,0) CNT	0.222	+0.006	2.94	0.38

The calculations show that the binding energy between the passivated Dia surface and the CNT is relatively weak. Bader charge analysis[44] reveals that the charge transfer between the CNT and Dia (100) is also limited, further indicating that their interaction is primarily driven by van der Waals forces. Notably, electrons are transferred to the CNT only when the surface is passivated with H, whereas in other passivation cases, electrons transfer from the CNT to the Dia. Figure 2 shows the charge transfer distribution, where the yellow and cyan regions represent charge accumulation ($\rho > 0$) and depletion ($\rho < 0$), respectively.[45,46] The results demonstrate that the type of passivation significantly affects the direction of charge transfer, providing a theoretical basis for modulating the electronic properties at the interface. Additionally, we performed detailed calculations and analyses for the 2 × 2 reconstructed surface, and the specific results are provided in Table S1 and Fig. S4.

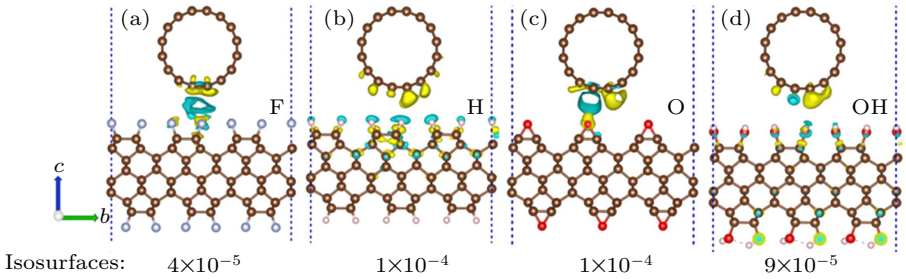


Fig. 2. Charge density difference isosurfaces for the hybrid structures of diamond (100)-2 × 1 surface and (8,0) carbon nanotube with four different capping terminations: (a) F-capping, (b) H-capping, (c) O-capping, and (d) OH-capping. Yellow and cyan regions represent electron accumulation and depletion, respectively.

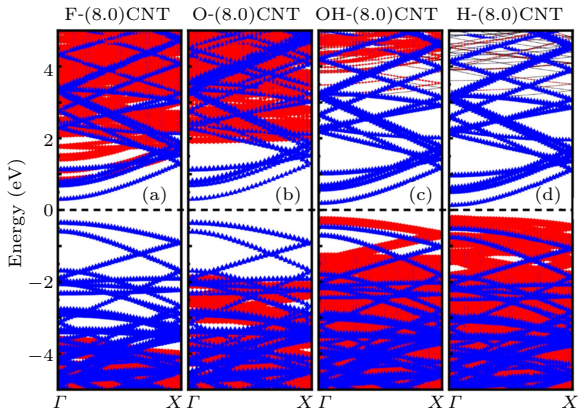


Fig. 3. Electronic band structures of the hybrid system consisting of a diamond (100)-2 × 1 surface and an (8,0) carbon nanotube with four different passivation species: (a) F-, (b) O-, (c) OH-, and (d) H-terminations. In all panels, the band structures are plotted along the high-symmetry path Γ–X in the Brillouin zone. The red lines represent the projected bands of the diamond component, and the blue lines represent those of the carbon nanotube component. The Fermi level is set to 0 eV (dashed line).

Based on the relaxed structure, the PBE functional was used to investigate the electronic band structures of the 2 × 1 reconstructed Dia (100) surface and carbon nanotube (CNT) heterostructures under different passivation treatments. Figure 3 illustrates the projected band structures of these heterostructures under various passivation conditions, where the red and blue lines represent the passivated Dia (100) surface and the (8,0) CNT, respectively. It can be clearly observed that all Dia/CNT heterostructures exhibit a direct bandgap, with the corresponding bandgap values listed in Table 1. It should also be noted that the heterostructure composed of F- and O-passivated Dia (100) surfaces with CNT belongs to the type-I heterostructure, and the bandgap is determined solely by the CNT (see Figs. 3(a) and 3(b)). (A type-I heterostructure refers to a band alignment configuration between two materials, where the CBM and VBM of one material completely enclose those of the other material, resulting in a nested band structure.) In contrast, the heterostructure constituted by the OH- and H-passivated Dia (100) surface with CNT belongs to the type-II heterostructure. Its band gap is determined by both the Dia (100) surface and CNT. Additionally, we per-

formed projected band structure calculations for the Dia (100) surface with a 2×2 reconstruction under different passivation treatments. The results are shown in Fig. S5 in supporting materials. Unlike the 2×1 reconstruction, the 2×2 reconstruction of the Dia (100) surface exhibits an indirect band gap under all passivation conditions. Specifically, the F-, O-, and OH-passivated Dia (100) surfaces with (6,2) CNT form type-I heterostructures, whereas the H-passivation leads to a type-II heterostructure. The bandgap data for these systems are presented in Table S1. For type-I heterostructures, both the CBM and VBM are provided by CNT. In type-II heterostructures, the CBM is contributed by CNT, while the VBM is primarily determined by the passivated Dia (100) surface.

To further investigate the impact of passivating atoms on the electronic properties of the CNT/Dia (100) heterojunction, the band shifts for the four passivation treatments are investigated by means of the vacuum level alignment method. Analysis of the electrostatic potential profile of the Dia (100)/CNT heterojunction reveals no notable difference in electrostatic potential between the CNT and the Dia (100) surface (see Fig. S6). Due to the absence of a potential difference, the heterojunction's band structure results from the direct superposition of Dia and CNT bands. Thus, the impact of passivation atoms on the heterojunction's band structure can be predicted by their influence on Dia's band structure. Further analysis reveals that passivation treatments significantly affect the band alignment of the heterostructure. For the heterostructure formed by CNT and F/O-passivated Dia (100) surfaces, a type-I band alignment is observed, whereas a type-II band alignment occurs in the OH/H-passivation cases. To accurately determine the CBO and VBO of the functionalized Dia (100)/CNT heterojunctions, we systematically investigated the band alignment for both type-I and type-II heterostructures. The band alignment results indicate that the electronic energy levels of these type-I and type-II heterostructures are in excellent agreement with the Anderson model. The band alignment equation of the Anderson model[47,48] is defined as

$$E'_{\mathrm{CBM}} = E_{\mathrm{CBM}} - E_{\mathrm{Evace}}, \tag{2}$$

$$E'_{\mathrm{VBM}} = E_{\mathrm{VBM}} - E_{\mathrm{Evace}}. \tag{3}$$

Here, E_{CBM}, E_{VBM}, and E_{Evace} represent the CBM, VBM, and vacuum levels, respectively, as directly calculated. E'_{CBM} and E'_{VBM} denote the positions of the CBM and VBM after vacuum level correction. The definitions of the CBO and VBO are given by

$$\mathrm{CBO} = \left|E'_{\mathrm{CBM-Dia}} - E'_{\mathrm{CBM-CNT}}\right|, \tag{4}$$

$$\mathrm{VBO} = \left|E'_{\mathrm{VBM-Dia}} - E'_{\mathrm{VBM-CNT}}\right|. \tag{5}$$

Here, CBO refers to the conduction band offset, while VBO refers to the valence band offset. $E'_{\mathrm{CBM-Dia}}$ and $E'_{\mathrm{VBM-Dia}}$ represent the corrected CBM and VBM positions for the Dia surface, while $E'_{\mathrm{CBM-CNT}}$ and $E'_{\mathrm{VBM-CNT}}$ correspond to the corrected CBM and VBM positions for the CNT surface. This result reveals the precise band alignment characteristics of the Dia (100)/CNT heterostructure under different passivation conditions, providing a theoretical basis for further tuning its electronic properties.

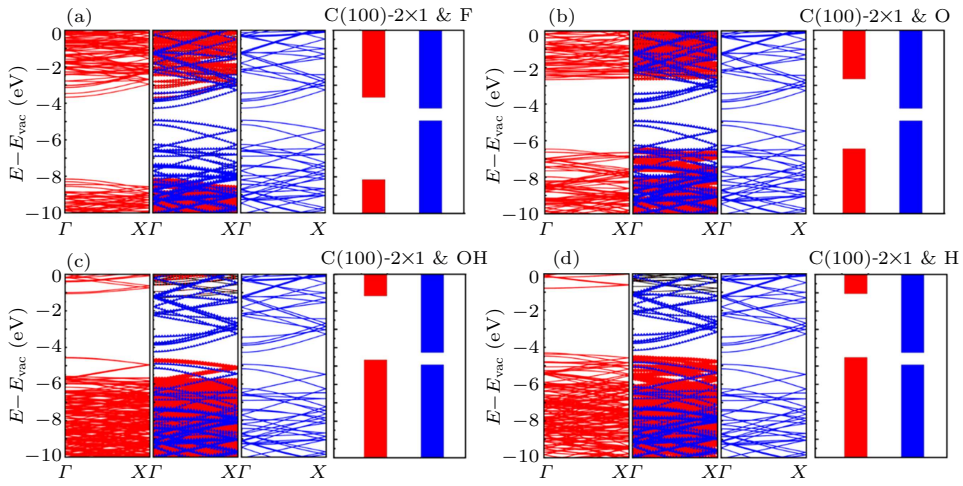


Fig. 4. The left figure shows the band structures of diamond (100)-2×1 (a) F, (b) O, (c) OH, and (d) H passivated systems, composite systems, and (8,0) carbon nanotubes under vacuum alignment. Red and blue lines represent the electronic contributions from diamond and carbon nanotube components, respectively. The right figure shows the corresponding vacuum-corrected band structures, where the red and blue regions represent the valence band and conduction band of diamond and carbon nanotubes, respectively.

Based on the aforementioned band alignment, the energy band diagram is illustrated in Fig. 4. Due to the practical requirements of CNT-FET devices, in this work we focus exclusively on type-I heterojunction structures. As shown in Figs. 4(a) and 4(b), the type-I heterojunctions are formed by F/O-passivation, with CBO values of 0.61 eV/1.61 eV and VBO values of 3.22 eV/1.53 eV, respectively. For sensor applications, the CBO and VBO at the gate are crucial for de-

vice performance. Larger CBO and VBO values could reduce electron-hole recombination and escape effects, thereby effectively suppressing the leakage current and electron tunneling phenomena. This, in turn, enhances the sensitivity and signal-to-noise ratio (SNR) of the sensor device.[49,50] Furthermore, larger CBO and VBO values can alleviate issues such as band bending and interface state density, which can reduce carrier loss and scattering, leading to lower power consumption and improved long-term device stability. Therefore, to optimize the performance of the Dia (100)/CNT type-I heterojunction system, it is essential to ensure that both the CBO and VBO are greater than 1.0 eV. This requirement ensures improved device performance and stability.

To obtain more accurate electronic properties, the HSE06 functional is utilized to refine the band structure of the Dia (100)/CNT heterojunction. As shown in Fig. 5, the HSE06 functional not only effectively corrects the band gap but also significantly alters the positions of the CBM and VBM. The CBO and VBO values obtained using the PBE functional are 0.61 eV and 3.22 eV, respectively, while those corrected by the HSE06 functional increase to 0.86 eV and 3.91 eV. In other words, the HSE06 functional leads to significant changes in both the CBO and VBO values. Generally, the HSE06 functional provides more accurate predictions of the CBO and VBO for real material systems, which is crucial for assessing their performance in sensor applications. For the type-I heterojunction, the introduction of HSE06 did not alter the heterojunction type. However, for the type-II heterojunction, the HSE06 correction leads to different outcomes. As shown in Fig. S7, the PBE calculation predicts the H-passivated Dia (100)/CNT heterojunction to be type-I, with CBO and VBO values of 3.18 eV and 0.28 eV, respectively. After HSE06 correction, the heterojunction transforms into a type-II heterojunction. Therefore, the HSE06 method not only adjusts the values of CBO and VBO but may also change the type of the heterojunction.

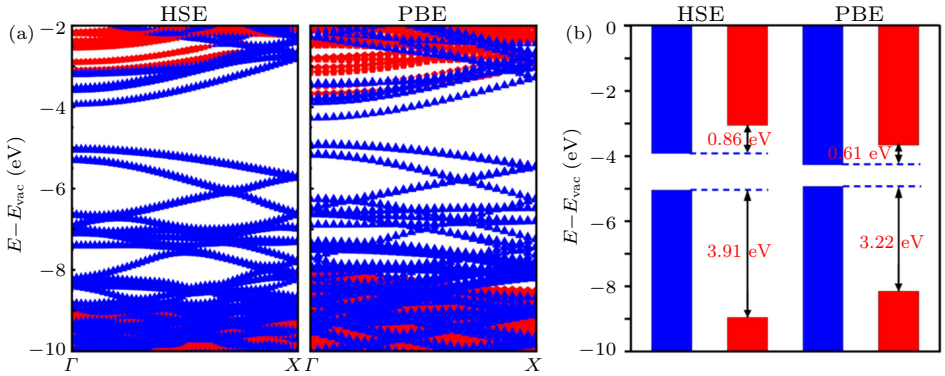


Fig. 5. (a) Band structures of Dia (100)-2 × 1 reconstruction and (8,0) CNT with F termination, calculated using both HSE06 and PBE methods, (b) along with alignment and correction. Red and blue indicate the contributions from diamond and carbon nanotubes, respectively.

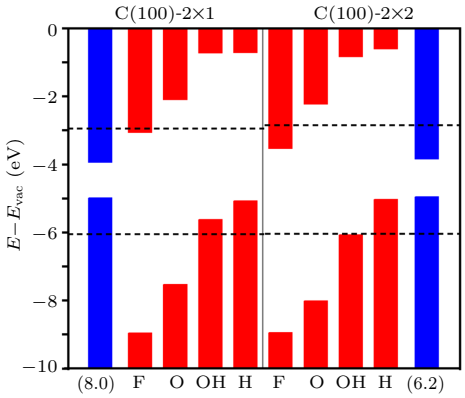


Fig. 6. The corrected alignment of Dia (100)-2 × 1 reconstruction & (8,0) carbon nanotubes and Dia (100)-2 × 2 reconstruction & (6,2) carbon nanotubes with four different passivation treatments, based on HSE06 calculations.

Given the results presented above, to obtain more accurate results, we recalculated the CBM and VBM positions for Dia (100) and CNT with different passivation treatments using the HSE06 functional and the vacuum level alignment approach. These recalculated results were used to reorder the band structures of the heterostructures. As mentioned earlier, for optimal device performance, the electronic structure should host a type-I heterojunction characterized by CBO and VBO offsets greater than 1.0 eV. From Fig. 6, it is clear that only three heterojunctions satisfy this requirement: O/OH-type passivation with a 2 × 2 reconstructed Dia (100) surface, and O-type passivation with both 2 × 2 and 2 × 1 reconstructed Dia (100) surfaces. Regardless of the surface reconstruction, the O-passivated structures exhibit CBO and VBO values significantly greater than 1.0 eV. Therefore, the heterojunction system formed by CNT and the O-passivated Dia (100) surface is the most reliable approach for designing Dia/CNT electronic devices.

4. Conclusion

In summary, we systematically investigated the electronic structure and band alignment of the reconstructed Dia (100) surface passivated with F, O, OH, and H, as well as its interaction with CNTs, using first-principles methods. The constructed heterostructures primarily consist of type-I and type-

II heterojunctions, which are consistent with the Anderson model. Our results demonstrate that surface passivation can effectively modulate the direction of charge transfer between the CNT and the Dia surface. Specifically, in the H-passivated Dia heterostructure, the CNT gains electrons, whereas in other passivation cases, electrons transfer from CNT to Dia. All heterostructures exhibit semiconductor behavior. After HSE06 corrections, not only do the CBO and VBO values change, but the heterojunction type may also shift. However, the electronic structure of the composite system can be predicted through vacuum energy level alignment by calculating only the individual electronic structures. Notably, for the O-passivated surface, the CBO and VBO of the heterostructure formed with CNT exceed 1 eV, regardless of the reconstruction type. This indicates effective confinement of electron-hole pairs in these systems, significantly reducing leakage current in related devices. The experimental integration of Dia (100)/CNT heterostructures, with their excellent thermal stability and appropriate lattice mismatch, shows great promise for nanoelectronic applications. Our work provides a feasible strategy for achieving large band offsets and valuable insights for developing high-power CNT-based field-effect transistors.

Acknowledgements

Project supported by the National Natural Science Foundation of China (Grant No. 52473258), the National Key Research and Development Program of China (Grant Nos. 2020YFA0714703 and 2022YFC2205003), the Technology Innovation Program of Hunan Province, China (Grant No. 2022RC3027), the Hunan Provincial Innovation Foundation of Postgraduate (Grant No. CX20230635), the Numerical computations were performed at the Hefei Advanced Computing Center, and the Key Project of Xiangtan Municipal Science and Technology Bureau (Grant No. ZX-ZD20240001).

References

[1] Shulaker M M, Van Rethy J, Hills G, Wei H, Chen H Y, Gielen G, Wong H S P and Mitra S 2014 *IEEE J. Solid-State Circuits* **49** 190
[2] Liu L, Han J, Xu L, Zhou J, Zhao C, Ding S, Shi H, Xiao M, Ding L, Ma Z, Jin C, Zhang Z and Peng L M 2020 *Science* **368** 850
[3] Lin Y, Cao Y, Ding S, Zhang P, Xu L, Liu C, Hu Q, Jin C, Peng L M and Zhang Z 2023 *Nat. Electron.* **6** 506
[4] Yang D, Hu J, Liu H, Li S, Su W, Li Q, Zhou N, Wang Y, Zhou W, Xie S and Kataura H 2017 *Adv. Funct. Mater.* **27** 1700278
[5] Xu L, Yang J, Qiu C, Liu S, Zhou W, Li Q, Shi B, Ma J, Yang C, Lu J and Zhang Z 2021 *ACS Appl. Mater. Interfaces* **13** 31957
[6] Franklin A D, Hersam M C and Wong H S P 2022 *Science* **378** 726
[7] Zhu Y, Lin W, Li D, Li L A, Lv X Y, Wang Q L and Zou G T 2023 *Chin. Phys. B* **32** 088101
[8] Liu Y, Ding S, Li W, Zhang Z, Pan Z, Ze Y, Gao B, Zhang Y, Jin C, Peng L M and Zhang Z 2024 *ACS Nano* **18** 19086
[9] McMorrow J J, Cress C D and Affouda C A 2012 *ACS Nano* **6** 5040
[10] Tong L, Wan J, Xiao K, Liu J, Ma J, Guo X, Zhou L, Chen X, Xia Y, Dai S, Xu Z, Bao W and Zhou P 2023 *Nat. Electron.* **6** 37
[11] Liang M, Yan H, Wazir N, Zhou C and Ma Z 2024 *Nanomaterials* **14** 1048
[12] Wang Z, Hemmetter A, Uzlu B, Saeed M, Hamed A, Kataria S, Negra R, Neumaier D and Lemme M C 2021 *Adv. Electron. Mater.* **7** 2001210
[13] Pendurthi R, Jayachandran D, Kozhakhmetov A, Trainor N, Robinson J A, Redwing J M and Das S 2022 *Small* **18** 2202590
[14] Wort C J H and Balmer R S 2008 *Mater. Today* **11** 22
[15] James M C, Fogarty F, Zulkharnay R, Fox N A and May P W 2021 *Carbon* **171** 532
[16] Gu L X, Yang K, Teng Y, Zhao W K, Zhao G Y, Fan K K, Feng B, Zhang R, Zheng Y D, Ye J D, Zhu S M, Tang K and Gu S L 2024 *Chin. Phys. B* **33** 098102
[17] Xin Y, Lu J, Li C, Luo Q, Li Z, Ke C and Xu X 2024 *Diam Relat. Mater.* **141** 110685
[18] Sakane S, Ishibe T, Yukawa Y and Nakamura Y 2023 *Diam. Relat. Mater.* **140** 110410
[19] Fedortchouk Y 2019 *Earth-Sci Rev.* **193** 45
[20] Qu W, Li W, Feng X, He Y, Pan W, Guo K, Li M, Tan M, Yang B and Wei H 2023 *Adv. Funct. Mater.* **33** 2213955
[21] Lin J, Huang R, Peng X, Zhang J, Zhang G, Wang W, Pan Z, Rao H and Zhong X 2024 *Adv. Mater.* **36** 2404561
[22] Feng X, Yuan X, Zhou J, An K, Zhu F, Wei X, Huang Y, Zhang J, Chen L, Liu J, Li C and Wei J 2025 *Mater. Sci. Semicond. Process* **186** 109008
[23] O'Donnell K M, Martin T L, Fox N A and Cherns D 2010 *Phys. Rev. B* **82** 115303
[24] Wang B, Zhao J, Hu Y, He Y, Rodionov N, Han J and Zhu J 2022 *Phys. Rev. B* **106** 184303
[25] Yang H X, Xu L F, Fang Z, Gu C Z and Zhang S B 2008 *Phys. Rev. Lett.* **100** 026101
[26] Jia S N, Li G X, Gao N, Cheng S H and Li H D 2023 *Chin. Phys. B* **32** 077301
[27] Wang B, He Y, Rodionov N and Zhu J 2023 *Mater. Today Phys.* **36** 101182
[28] Yan L, Sun Q and Jia Y 2008 *J. Phys.: Condens. Matter* **20** 225016
[29] Horner D A, Sternberg M, Zapol P and Curtiss L A 2011 *Diam. Relat. Mater.* **20** 1103
[30] Kang J, Tongay S, Zhou J, Li J and Wu J 2013 *Appl. Phys. Lett.* **102** 012111
[31] Fan Y, Hou K, Wang Z, He T, Zhang X, Zhang H, Dong J, Liu X and Zhao M 2011 *J. Phys. D: Appl. Phys.* **44** 095405
[32] Cañas J, Reyes D F, Zakhtser A, Dussarrat C, Teramoto T, Gutiérrez M and Gheeraert E 2022 *Nanomaterials* **12** 4125
[33] Sque S J, Jones R, Öberg S and Briddon P R 2007 *Phys. Rev. B* **75** 115328
[34] Kresse G and Furthmüller J 1996 *Phys. Rev. B* **54** 11169
[35] Perdew J P, Burke K and Ernzerhof M 1996 *Phys. Rev. Lett.* **77** 3865
[36] Polat E O, Balci O, Kakenov N, Uzlu H B, Kocabas C and Dahiya R 2015 *Sci. Rep.* **5** 16744
[37] Jun L, Juan Z, Shengling D, Boryssenko A O, Joyner V M and Huang Z R 2010 *J. Comput. Chem.* **29** 2044
[38] Kresse G and Joubert D 1999 *Phys. Rev. B* **59** 1758
[39] Grimme S 2006 *J. Comput. Chem.* **27** 1787
[40] Blöchl P E, Jepsen O and Andersen O K 1994 *Phys. Rev. B* **49** 16223
[41] Hine N D M, Frensch K, Foulkes W M C and Finnis M W 2009 *Phys. Rev. B* **79** 024112
[42] Perdew J P, Ernzerhof M and Burke K 1996 *J Chem. Phys.* **105** 9982
[43] Henderson T M, Paier J and Scuseria G E 2010 *Phys. Status Solidi (b)* **248** 767
[44] Sanville E, Kenny S D, Smith R and Henkelman G 2007 *J. Comput. Chem.* **28** 899
[45] Ou Q, Zhang Y, Wang Z, Yuwono J A, Wang R, Dai Z, Li W, Zheng C, Xu Z Q, Qi X, Duhm S, Medhekar N V, Zhang H and Bao Q 2018 *Adv. Mater.* **30** 1705792
[46] Chiah S B, Zhou X, Chandrasekaran K, Shangguan W Z, See G H and Pandey S M 2005 *Appl. Phys. Lett.* **86** 202111
[47] Koda D S, Bechstedt F, Marques M and Teles L K 2018 *Phys. Rev. B* **97** 165402
[48] Anderson R L 1960 *IBM J. Res. Dev.* **4** 283
[49] Rajan N K, Routenberg D A and Reed M A 2011 *Appl. Phys. Lett.* **98** 264107
[50] Zhang L, Li B, Li H, Gu G and Wang X 2024 *IEEE Photonics J.* **16** 7800609